Thallium Long-Term Fate from Rock-Deposit to Soil: The Jas Roux Sulfosalt Natural Analogue

Jérôme Rose, Perrine Chaurand, Cédric Dentant, Bernard Angeletti, Daniel Borschneck, Isabelle Kieffer, Olivier Proux, Richard Bonet, Mélanie Auffan, Clément Levard, et al.

▶ **To cite this version:**

Jérôme Rose, Perrine Chaurand, Cédric Dentant, Bernard Angeletti, Daniel Borschneck, et al.. Thallium Long-Term Fate from Rock-Deposit to Soil: The Jas Roux Sulfosalt Natural Analogue. ACS Earth and Space Chemistry, 2023, 7 (10), pp.1848-1857. 10.1021/acsearthspacechem.3c00021 . hal-04230624

HAL Id: hal-04230624
https://amu.hal.science/hal-04230624

Submitted on 21 Nov 2023

HAL is a multi-disciplinary open access archive for the deposit and dissemination of scientific research documents, whether they are published or not. The documents may come from teaching and research institutions in France or abroad, or from public or private research centers.

L'archive ouverte pluridisciplinaire **HAL**, est destinée au dépôt et à la diffusion de documents scientifiques de niveau recherche, publiés ou non, émanant des établissements d'enseignement et de recherche français ou étrangers, des laboratoires publics ou privés.

Thallium long-term fate from rock-deposit to soil: the Jas Roux sulfosalt natural analogue

Jérôme Rose[a]; Perrine Chaurand[a]; Cédric Dentant[b,c]; Bernard Angeletti[a]; Daniel Borschneck[a]; Isabelle Kieffer[d]; Olivier Proux[d]; Richard Bonet[b]; Mélanie Auffan[a]; Clément Levard[a]; Till Fehlauer[a]; Blanche Collin[a]; Emmanuel Doelsch[a,e,f]*

[a]CNRS, Aix Marseille Univ, IRD, INRAE, CEREGE, 13545 Aix-en-Provence, France

[b]Ecrins National Park, 05000 Gap, France

[c]Univ. Grenoble Alpes, CNRS, Sciences-Po Grenoble, Pacte, Grenoble, 38000, France

[d]Univ. Grenoble Alpes, UAR CNRS 832, OSUG, 38041 Grenoble, France

[e]CIRAD, UPR Recyclage et Risque, 34398 Montpellier, France

[f]Recyclage et Risque, Univ. Montpellier, CIRAD, 34398 Montpellier, France

*Corresponding author: rose@cerege.fr

KEYWORDS: high-tech metal, oxidation, national park, critical element, speciation, XAS.

GRAPHICAL ABSTRACT

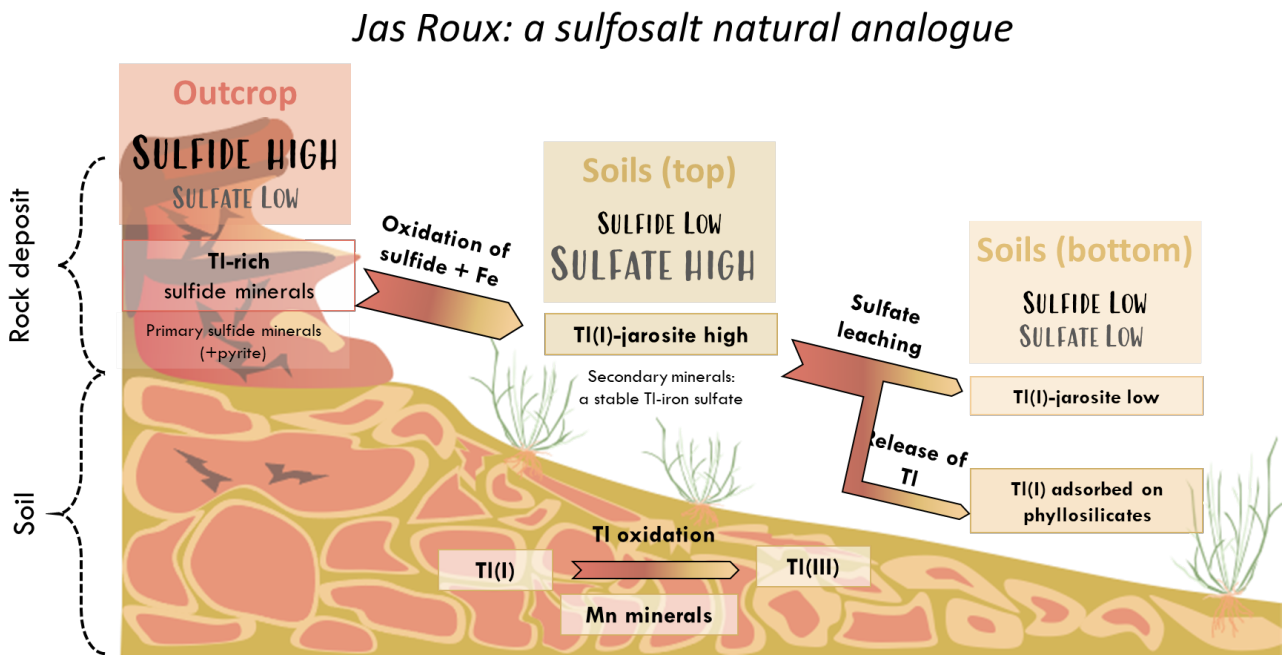

ABSTRACT

Inorganic contaminant release resulting from mining activities can impact surrounding ecosystems. Ores formed by primary sulfide minerals produce sulfuric acid after mineral oxidation which is the driving force of metal release. Yet secondary metal sulfates may form and play a crucial role in controlling the metal fate. In the case of thallium (Tl), it has been shown that in natural Tl-rich sulfide deposits and those found in mining areas, Tl can be trapped by Tl-jarosite (Tl-rich iron sulfate) and dorallcharite ($TlFe_3(SO_4)_2(OH)_6$). Our Tl speciation characterization results have generated novel insight into the long-term behavior of this metal derived from a unique natural hotspot—the Jas Roux site (France). The biogeochemical cycle of the soil ecosystems of Jas Roux dates back almost 15000 years ago and has now reached a steady state. A chemical gradient was found in soils across the toposequence underlying the Jas Roux outcrop. X-ray absorption spectroscopy revealed that Tl was mainly present in secondary minerals at the top of the studied zone. Oxidative dissolution of Tl-rich

sulfide minerals and pyrite accounts for the presence of Tl-jarosite in soils, either by direct formation in soils or by gravity erosion from the outcrop. The Tl-jarosite quantity was found to decrease from the top to the bottom of the toposequence, probably due to sulfate leaching. Released Tl likely adsorbed on phyllosicates such as illite or muscovite and a fraction of Tl was found to have oxidized into Tl(III) along the toposequence.

INTRODUCTION

Human activities, especially mining, lead to the release of many inorganic environmental contaminants. Globally, the highest tonnages of common metals such as lead, copper and zinc derive from ores containing primary sulfide minerals. These ores are accompanied by iron sulfide minerals (marcasite FeS_2, pyrite FeS_2 and pyrrhotite $Fe_{1-x}S$) which produce sulfuric acid by oxidation and hydrolysis. When leached, this acid subsequently triggers the release of metals and metalloids from extracted ores and mine wastes. However, in this acidic environment, secondary metal sulfates may form after sulfide oxidation, which can play a crucial role in affecting the storage and transport of released metals[1].

Thallium (Tl) is a low-abundance element (average crustal abundance <0.8 $mg.kg^{-1}$ [2]) with an average concentration of 0.29 $mg.kg^{-1}$ in French soils[3]. In soil and rock, Tl can be hosted by many different minerals. Almost hundred Tl-bearing minerals are known[4]. However, Tl generally occurs in three main types of minerals, namely sulfide minerals, secondary sulfate minerals and silicate minerals such as feldspars or phyllosilicates through the isomorphic substitution of K^+ [3,5,6]. Natural Tl-rich deposits are rare. Only a few have been identified at different sites, including Allchar (Macedonia)[7], Lengenbach quarry (Switzerland)[5,8], Skrikerum (Sweden), Lanmuchang (China)[9,10] and Jas Roux (France)[11]. In the latter deposits, Tl is mainly associated with sulfide minerals and its mobility is driven by oxidative dissolution processes[4].

Due to its specific electronic properties, Tl is used in different modern high technology applications, such as semiconductors, superconductors, fiber optics and thermoelectric conversion[12–17]. However, Tl is just as toxic to mammals as mercury, for instance[18–20]. Thallium can occur under two oxidation states, with Tl(I) being thermodynamically more stable than Tl(III) and relatively less toxic. Tl(I) is more mobile than Tl(III) in surface ecosystems [10,20]. Tl(I) was long considered to be the only form occurring

63 in the critical zone, yet low Tl(III) amounts were subsequently found in rivers, waste waters, soils and
64 plant tissues[5,21–25].

65 In the vicinity of Tl sulfide ores and/or mines, secondary Tl-sulfate phases can precipitate and control
66 Tl(I) free ions in solution. Two main Tl(I)-sulfate minerals have been found, namely lanmuchangite
67 ($TlAl(SO_4)_2 \cdot 12H_2O$) and dorallcharite ($TlFe_3(SO_4)_2(OH)_6$). While lanmuchangite is only stable at
68 acidic conditions, dorallcharite—a jarosite analogue in which K^+ has been fully replaced by Tl(I)
69 (jarosite = $KFe_3^{3+}(SO_4)_2(OH)_6$)—is less soluble at > 5.5 pH[26]. Dorallcharite and Tl(I)-jarosite could
70 therefore act as a trap for Tl since it has been identified in various Tl-rich sulfide deposits, namely
71 Lanmuchang, Allchar and Tuscany[7,27], and in Tl polluted areas[28,29]. However, do dorallcharite and Tl-
72 jarosite remain stable during soil weathering by meteoric water? Besides sulfate minerals, Tl can be
73 hosted by other minerals: silicates in which Tl substitutes K, or Mn oxide minerals via Tl(I) oxidation
74 to Tl(III). Do those Tl-bearing phases also occur after long-term evolution of soils in the vicinity of Tl
75 sulfide-rich or polluted sites?

76 Voegelin et al[5] reported Tl speciation in a natural soil developed from mineralized carbonate rock
77 (Erzmatt site). In addition to the presence of Tl-jarosite, the study revealed for the first time the
78 important role of Tl(I) associated with illite and Tl(III) associated with manganese minerals in
79 quantifying Tl bioavailability. As the initial source term no longer exists, it is difficult to assess the
80 evolution of Tl-bearing minerals from the supposed parent sulfide minerals and their long-term
81 transformation in soils.

82 Assessing the long-term fate of Tl in soil whether contaminated or pristine might be crucial to better
83 remediate and predict Tl transfer from geogenic environments into living organisms and the food
84 chain. Natural analogues provide an excellent opportunity to study the long-term fate and complex
85 geochemical cycling of Tl.

The Jas Roux site is located in Ecrins National Park in La Chapelle-en-Valgaudemar valley, France (Figure 1A), and is a unique unimpaired site with detectable amounts of Tl[11]. The rock deposit is hosted by a Triassic sedimentary series of the Morges syncline[11,30]. It has been investigated by Mantienne[30], Johan and Mantienne[11] and Favreau et al[31]. The geological setting and mineralogical composition were extensively studied. The rock deposit exhibits a unique mineralogy, including pyrite (FeS), stibnite (Sb_2S_3), sphalerite (ZnS), realgar (AsS), other Ag, Pb-rich sulfide minerals such as jasrouxite[32], along with rare Tl minerals like pierrotite ($TlSb_3As_2S_8$), routhierite ($Tl(Cu,Ag)(Hg,Zn)_2(As,Sb)_2S6$) and chabourneite ($(Tl, Pb)_{23}(Sb,As)_{91}S_{147}$)[33,34]. Some parts of the deposit exhibit alteration facies (Figure S1), and oxidized sulfate minerals have been detected. For instance, jarosite was found, while dorallcharite was identified as a Tl-rich secondary mineral[30,31]. These minerals occur in a small outcrop structured with five blocks separated by NW-SE oriented faults at 2170 to 2300 m elevation. The deposit covers less than 10000 m^2, with a 45° slope that is subject to heavy erosion, causing the fall of rock debris which ends up downstream. This process leads to the transfer of Tl from upstream to downstream soils, as shown by Fehlauer et al[35]. The current functioning of the Jas Roux soil ecosystem is the result of long-term processes. The final exhumation of the South-East part of the Pelvoux crystalline massif occurred in the late Miocene[36], but the current ecosystem is a result of the colonization by living organisms after the last glacial maximum. Based on ^{10}Be dating, it was estimated that the glacial retreat in Gioberney valley, close to Jas Roux, occurred 15 ± 1 ky[37].

Although the chemical composition of soils at the top of the toposequence has been determined, soil evolution from the top to the bottom of the toposequence and the Tl speciation pattern have yet to be clarified.

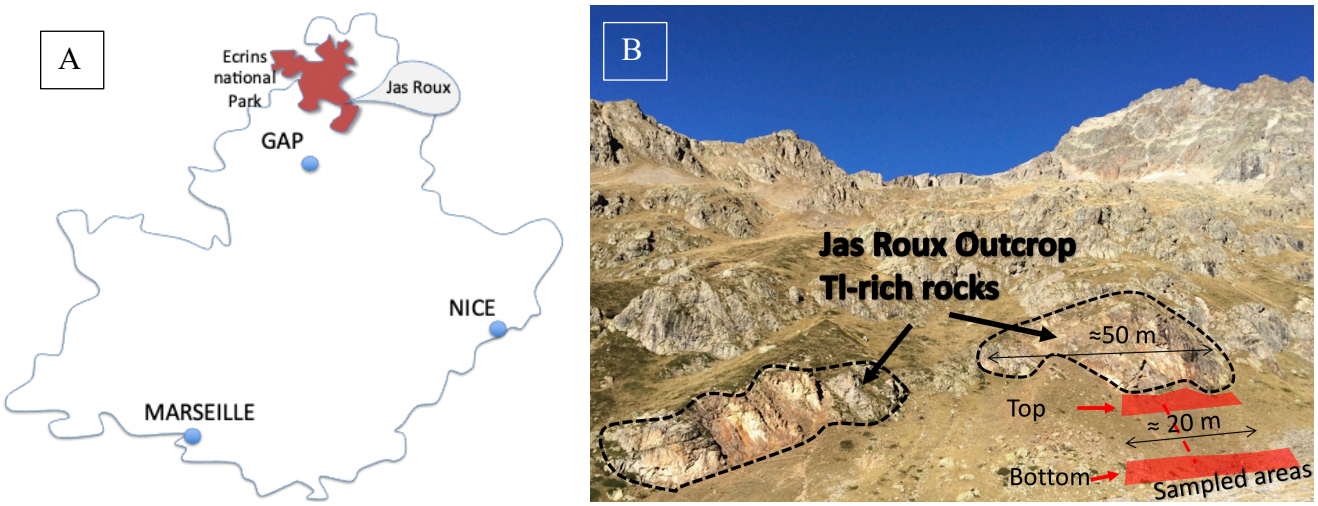

107

***Figure 1**: A) Location of the site, B) the Jas Roux deposit with the sampling zones at the top and bottom of the slope below the Tl-rich outcrop.*

108 The main aim of this study was to address the fate of Tl in soils developed below the Jas Roux
109 outcrop. The working hypothesis was that a Tl concentration gradient from the top to the bottom of
110 the toposequence is associated with a significant change in Tl speciation. The specific objectives were
111 to determine: i) under which form Tl is transferred from the rocky outcrop to the soil below, ii) whether
112 stable Tl minerals such as Tl-jarosite are formed in Jas Roux soils to serve as a Tl trap throughout the
113 toposequence, and iii) whether Tl(III) can be formed in soils beneath the rocky outcrop.

114

115

1) MATERIALS AND METHODS

1) Soil samples

The Jas Roux site in Ecrins National Park is protected and sampling is forbidden. A waiver was granted by the National Park to allow for a limited number of soil samples under their supervision.

The selected area below the outcrop (Figure 1B) was sampled from the top to the bottom of the toposequence. The developed soil was just a few tens of centimeters thick. The upper soil horizons contained many rock fragments from the outcrop. Furthermore, it is hard to sample soils remote from plants because of the substantial vegetation cover. We sampled soils in the vicinity of three plant species so as to assess their potential impact on the physicochemical soil properties. The top 10 cm soil layer was sampled near the identified plants, i.e. fescue, saxifrage and bedstraw. Soil samples were divided in two sets for chemical and X-ray based analysis (see below).

Fresh soils were dried for 48 h at 40°C and then sieved at 2 mm to recover the fine fraction according to the NF-ISO-11464 standard. A portion of the sieved soils was ground very finely in a Mixer Mill MM-400 (Retsch®) with ZrO_2 beads in 25 mL bowls. The grinding time was 150 s at 20 Hz frequency. A first set of ground soils were stored at -80°C prior to XAS analysis, while a second set was set aside for chemical analysis. The total chemical element content was determined for each sample (0.1 g) after soil digestion. Digestion is achieved by adding 1.5 mL HNO_3 to 0.1 g of powder in Teflon beakers. 3 mL HCl and 0.5 mL HF were then added according to the NF-X31-147 standard. The last digestion step was carried out in a microwave oven (MLS-UltraWave Thermo-Scientific). The sieved soils were deposited on scotch tape on an XRF sample holder before micro-XRF analysis.

2) Soil pH

The soil pH was determined according to the NF-ISO-10390:1994 standard[38]. The measurements were carried out in a 5 mL soil suspension obtained with 1 g of 2 mm sieved soil and ultrapure water

(18.2 MΩ·cm). The suspension was stirred for 5 min at 80 rpm on an IKA® 10-digital Roller Shaker then left to settle for 2 h. A multimeter (Hanna Instruments Hl-2550) was used for pH measurement.

3) *In situ* chemical analysis for sample preselection:

A handheld X-ray fluorescence spectroscope (XRF-Bruker Tracer®) was used on-site for fast non-destructive analysis directly on the soil so as to directly determine the metal plume below the deposit while optimizing the selected sample number (Figure S2).

4) Chemical analysis

The major elements (Mg, Al, Si, K, Ca, Fe) were analyzed using the inductively coupled plasma atomic emission spectrometry (ICP-AES) method (ICP-Perkin-Elmer 4300 DV). Digested samples were introduced with the fast autosampler ESI SC-4 DX-FAST. Inductively coupled plasma mass spectrometry (ICP-MS) was used (Perkin-Elmer Nexion 300x quadrupole) to quantify minor and trace elements (V, Mn, Zn, As, Sr, Ag, Sb, Cs, Ba, Tl, Pb). Soil samples were diluted prior to analysis to avoid saturation of the instrument. Multi-element standards CCS4, CCS5 and CCS6 (Inorganic Ventures, USA) diluted in 2% HNO_3 were used to obtain the ICP-MS calibration curves.

5) Statistical analysis

Statistical significance of differences between elemental concentrations of soils on top and the bottom of the toposequence were assessed using the Mann-Whitney U-test. The tests were performed using the Real-Statistics-Resource-Pack software package (Copyright (2013–2020) Charles Zaiontz. www.real-statistics.com). Statistical significance was set at $p<0.05$ for all tests.

6) Mineralogical analysis

Soil mineralogy was determined by X-ray diffraction (XRD) using an X'Pert-Pro PANalytical X-ray diffractometer equipped with a cobalt anode (λ=1.79 Å) and operating at 40 kV and 40 mA.

7) Hyperspectral chemical mapping by X-ray fluorescence microscopy

Hyperspectral chemical mapping was performed by X-ray fluorescence microscopy (micro-XRF) with a micro-XRF (XGT-7000 Horiba) equipped with an Rh X-ray source (50 kV, 1 mA). This enabled characterization of the spatial distribution of elements from Na to U and the identification of element co-localizations. 10 and 100 μm X-ray spot sizes were used for soil samples. By combining K ($11<Z<43$) and L ($Z>43$) X-ray emission lines, all elements with $Z>11$ could be detected with a sensitivity ranging from about 50 mg/kg to a few % mass.

The Fiji version of ImageJ software was used for chemical image analysis[39]. The co-localization procedure was performed with the Coloc2-plugin (https://imagej.net/Coloc_2) based on the pixel intensity correlation. Coloc2 calculates a variety of co-localization parameters such as the Pearson coefficient and the Manders correlation. The background of each element channel was removed. The Coloc2-plugin was implemented with bisection threshold regression on the entire image (128 x 128 px) or on selected regions of interest (ROI).

8) X-ray absorption spectroscopy for Tl speciation analysis

Thallium L_3-edge XAS spectra were obtained on the FAME beamline (ESRF Synchrotron, Grenoble, France) using a Si(220) monochromator. Freeze-dried or frozen-hydrated (-80°C) samples were powdered at -80°C and analyzed at 8-10 K to avoid sample beam damage. Measurements were performed in fluorescence mode with a 30-element Ge solid-state detector (SSD). A Gallium foil filter was used to avoid detector saturation due to the X-ray fluorescence of the matrix mainly due to As concentrations 10 times higher than the Tl concentration. On this beamline and using an SSD, XAS spectra can be measured with a sensitivity range from about 10 mg/kg to a few % mass[40]. Each final spectrum was the average of at least five scans of different zones of the same sample, and the standard deviation of these scans was used to assess the XAS signal variability. Energy calibration was performed using a metallic Se reference foil recorded simultaneously with the samples for which the

185 K-edge was at the same energy level as the Tl L_3 edge. The absorption edge was defined at 12658 eV.
186 Data reduction was performed using Athena software[41] and the MAX package[42]. Spectra were scanned
187 from 12600 to 13200 eV. This energy range was limited by the presence of other elements such as Pb
188 (L_3 edge at 13035 eV). XAS analysis was thus limited to the study of the X-ray absorption near edge
189 structure (XANES) and the lower energy zone of extended X-ray absorption fine structures (EXAFS),
190 thereby providing information on the valence state, the site geometry of Tl, as well as the nature of the
191 ligands.
192 Seventeen XAS spectra composed the spectral library of reference compounds (Table S1) used for
193 principal component analysis (PCA) and linear combination fitting (LCF). PCA is a multivariate
194 analysis technique that can be used to determine the lower number of independent components
195 (principal components) needed to reproduce the experimental spectra dataset. The LCF sensitivity
196 using reference compounds ranged from 5 to 20%[43]. PCA analysis of the soil spectra revealed that the
197 variance could be explained by a maximum of three components (Figure S3). A maximum of three
198 spectra from the reference database could therefore be used to fit the Jas Roux sample spectra via LCF.
199 During the fitting, the weight of each reference compound was restricted to between 0 and 1 without
200 forcing the sum to equal 100%.
201 One reference compound was used at the start of the fitting procedures and additional compounds
202 were added only if the fit residue was improved by >30% and was higher than the spectrum variability
203 calculated from the different scans per sample. One example is outlined in Figure S5. The relative
204 goodness-of-fit between the data and the model was represented by the residual factor (R-factor).

205 **9) Sensitivity of the XAS reference compound database to the Tl speciation**

206 The sensitivity of XAS in differentiating a high variety of Tl-species was investigated. The details
207 are given in the Supporting Information. In summary, the spectra of the 17 reference compounds
208 (Figure 4A & B) enabled us to distinguish Tl(I) and Tl(III) compounds via the position of the main

209 absorption line (Figure 4A), as well as a pre-edge feature at 12658.8 eV in the case of Tl(III). The
210 spectra of all Tl(I)-reference compounds also differed in terms of their oscillation amplitudes (high
211 amplitude for Tl(I) -jarosite, Tl_2SO_4 and Tl^+ adsorbed on illite and low for the others (Figure 4B)) and
212 the slight differences in their white line positions. The spectrum of Tl(I) adsorbed on illite exhibited a
213 positive oscillation at 12720 eV (Figure 4B), while the oscillations were negative for the others.
214

2) RESULTS AND DISCUSSION

1) Physicochemical gradient in the soil toposequence below the outcrop

The XRD soil mineralogical analysis findings at the top of the toposequence (Figure 2A) indicated the presence of abundant non-site-specific silicate minerals such as muscovite, orthoclase and quartz, as well as carbonate minerals such as calcite and dolomite. XRD also revealed the original features of the site, including the presence of soilborne barite (barium sulfate), jarosite (iron sulfate) and pyrite (iron sulfide) while confirming the results of Fehlauer et al.[35] concerning the top of the toposequence. Iron sulfides were highly abundant in the Jas Roux deposit[11] and were found to have been transferred to the soil below the outcrop. Jarosite was detected in soils. Its presence in the soil samples could be explained by pyrite oxidation in the soils or gravity erosion from the outcrop. Mineralogical analysis of soils sampled at the bottom of the toposequence revealed a similar mineral assembly pattern (Figure 2B). The presence of primary sulfide mineral confirmed the transfer of minerals via falling rocky debris due to mechanical erosion. At this stage, XRD only provided qualitative information regarding the presence of mineral phases—no quantitative information was obtained for comparison. Other parameters such as the pH and chemical composition revealed differences between soils at the top and bottom of the toposequence.

The soil pH at the top of the toposequence was 6.5±0.20 (n=5), which was similar to the values reported by Fehlauer et al.[35] (6.8±0.3 (n=10)), while the pH was lower at the bottom (5.6±0.18; n=5). There could have been many possible causes for the lower pH at the bottom, but they could not be determined at this stage. For example, sulfide oxidation undoubtedly causes soil acidification, yet the presence of carbonate minerals such as calcite could partially offset this phenomenon. The decreased calcite content at the bottom (XRD and decreased Ca level (Table 1) could thus explain why the pH was significantly more acidic. Other phenomena, such as micro-organism activity, could also partly contribute to the pH variation from the top to the bottom of the toposequence.)

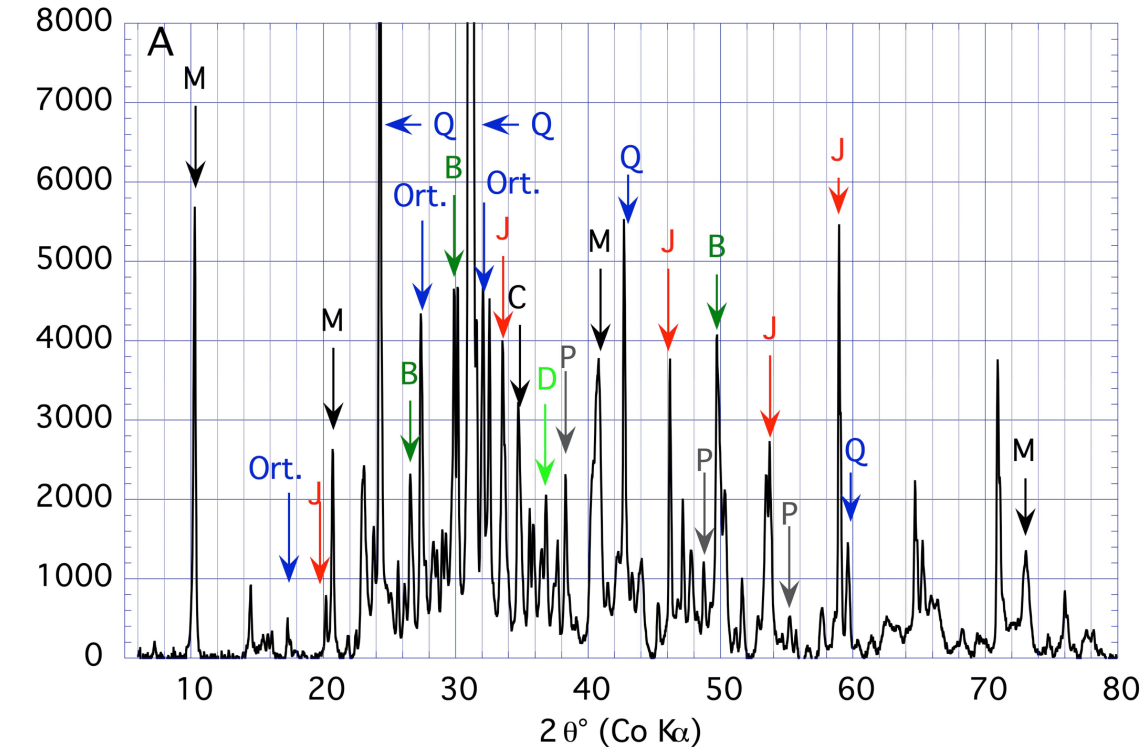

239

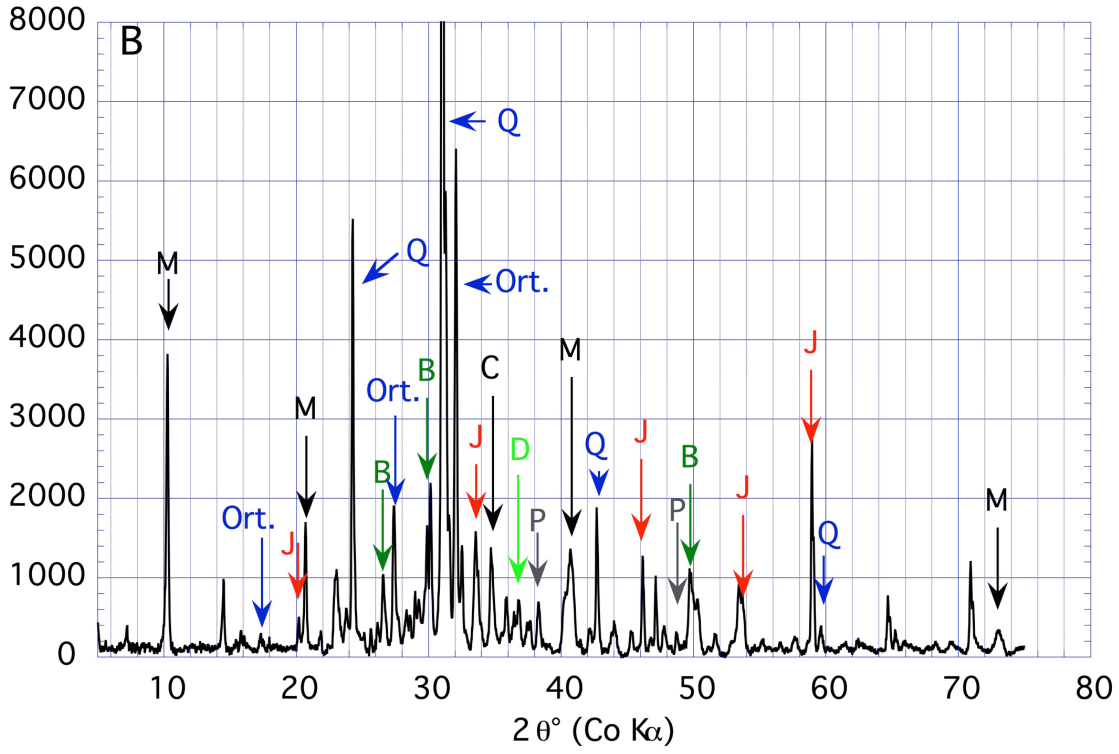

240

Figure 2: *X-ray diffractograms of the soil at: A) the top and B) the bottom of the selected areas below the outcrop (Q=quartz, Ort=orthoclase, M=muscovite, B=barite P=pyrite J=jarosite, C=calcite, D=dolomite). Intensity: arbitrary unit*

241 The chemical composition (Table 1) of the soils determined by ICP-AES and ICP-MS also, for the
242 first time, highlighted significant quantitative changes in major and minor elements along the
243 toposequence. While Mg, Al, Si, K, Ca, V, Mn and Cs concentrations did not statistically vary, the Fe,
244 Zn, As, Sr, Ag, Sb, Ba, Tl and Pb concentrations markedly decreased as function of the distance from
245 the source (outcrop). Note that the presence of different plant species did not affect the soil chemical
246 composition at the top or bottom of the toposequence. The decreased Fe concentration from 86
247 005±26 385 $mg.kg^{-1}$ at the top to 42 400±8 720 $mg.kg^{-1}$ at the bottom, and the decreased Ba
248 concentration from 53 020±23 190 $mg.kg^{-1}$ at the top to 24 080±22 090 $mg.kg^{-1}$ at the bottom indicated
249 a lower amount of primary minerals (pyrite and barite) from the outcrop source at the bottom of the
250 toposequence

251 In the case of Tl, a significant decrease of the concentration of this element was documented for the
252 first time in soils from the top (565±195$mg.kg^{-1}$) to the bottom (182±49 $mg.kg^{-1}$) of the toposequence.
253 This decrease could have been related to the reduction in the amount of primary minerals from the
254 source, as suggested by the decreased Fe and Ba concentrations, but it could also have been related to
255 higher weathering and leaching of soil minerals and to ongoing Tl chemical and mineralogical
256 transformation. The soil Tl concentration range was high compared to the average crustal abundance
257 (< 0.8 $mg.kg^{-1}$ [2]). These chemical analyses confirmed the results obtained by Fehlauer et al.[35] at the top
258 of the toposequence. Compared to other natural analogue sites, the Tl concentration was lower than at
259 the Erzmatt site, where it reached up 6000 $mg.kg^{-1}$ [5], and lower than in soils below the abandoned
260 Allchar mine, where it reached 20 000 $mg.kg^{-1}$ for an average of 660 $mg.kg^{-1}$ in 134 soils[7].
261
262
263
264

Table 1: Chemical composition (± standard deviation) of soils at the top and bottom of the study zone below the outcrop. (significant differences between top and bottom)*

$mg.kg^{-1}$	Soils at the top) (n=14)	Soils at the bottom (n=6)
Mg	11 940±16 550	6 070±3 570
Al	32 929±8 784	33 941±4 549
Si	132 339±24 451	118 043±22 279
K	33 445±3 380	30 140±7 510
Ca	140 130±185 201	36 542±76 029
V	100±14	94.4±20
Mn	2 250±1 140	2 410±645
Fe*	*86 005±26 385	42 400±8 720
Zn*	*832±327	422±59
As*	*3 810±1 670	816±243
Sr*	*949±550	390±311
Ag*	*20±13	4.2±1.4
Sb*	*2 160±1 000	361±168
Cs	14.4±5.0	14.5±2.9
Ba*	*53 020±23 190	24 080±22 090
Tl*	*565±195 (max 702)	182±49 (max 280)
Pb*	*385±190	137±19

2) Qualitative identification of Tl-bearing minerals in soils

Although jarosite was a clear Tl-bearing phase candidate, XRD failed to identify minerals containing Tl in soils. This suggests that Tl-minerals were present in scant amounts, with an ill-ordered structure or, as we assumed, that Tl speciation was more complex (i.e. Tl(I) substitution in minerals). Figure 3 presents a micro-XRF chemical image of a 2.56x2.56 mm^2 zone of one soil from the top zone, which illustrates the co-localization of Tl with other elements and possible Tl-bearing phases.

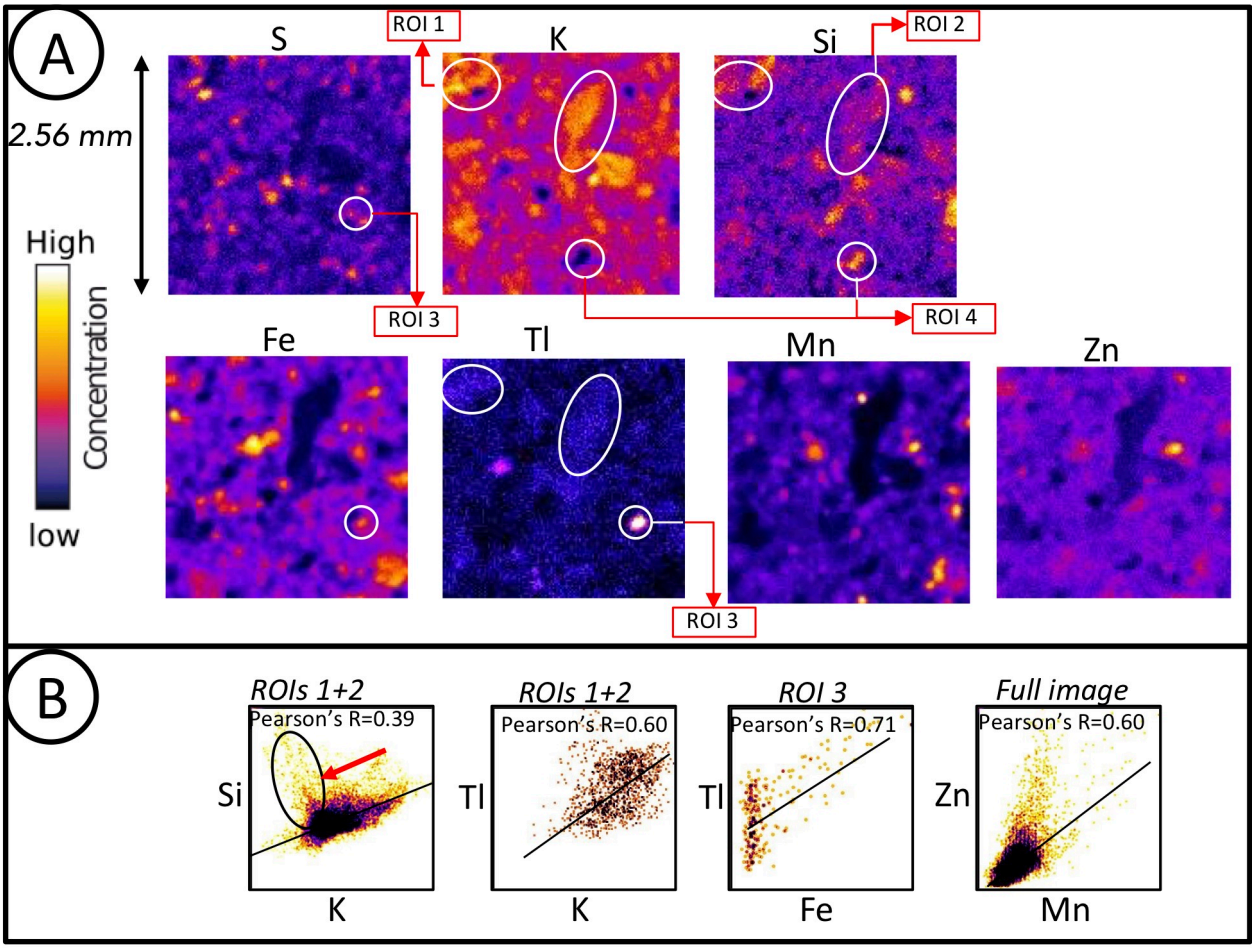

273

***Figure 3**: A) micro-XRF elemental maps of a soil from the top of the toposequence. The map size is 2.56 x 2.56 mm² (20 µm pixel size). Several element colocalization zones (regions of interest [ROI]) are highlighted: ROI 1&2 for K, Si and Tl, ROI 3 for S, Fe and Tl, ROI 4 for Si. B) 2D intensity diagram with co-localization Pearson's coefficient obtained using the Coloc2-plugin on selected ROIs and the full image for the Zn-Mn 2D diagram.*

274 The K and Si co-localization pattern (ROIs 1&2, Figure 3A) was consistent with the presence of
275 muscovite, a phyllosilicate mineral identified by XRD. The Pearson's coefficient (Figure 3B) was a
276 bit low and may have been due to the noise level on the Si image and the presence of an Si-rich zone
277 not correlated with K such as quartz revealed by XRD (e.g. ROI 4, Figure 3A). The Tl elemental map
278 suggests a relatively high XRF intensity associated with the muscovite zones (K and Si co-
279 localization). The Tl-K intensity diagram of the K-rich ROIs 1&3 and the high Pearson's coefficient
280 confirmed the co-localization of Tl with muscovite (Figure 3B). It has been shown that Tl can be
281 adsorbed to illite[6], a phyllosilicate mineral very similar to muscovite. Besides, the Tl elemental map
282 revealed a highly heterogeneous distribution and a hotspot in a Fe- and S-rich zone (ROI 3). This could

283 have been related to the presence of iron sulfide or iron sulfate minerals since XRF is not sensitive to
284 the redox state of elements. Although Tl-Fe sulfide minerals are known to exist (picotpaulite ($TlFe_2S_3$),
285 raguinite (TlFeS), etc.), none of them were identified at the Jas Roux deposit. However, using an
286 electron microprobe, Johan and Mantienne[11] found that pyrite contained 0.07% Tl. Jarosite may also
287 contain Tl. The formation of dorallcharite ($TlFe_3(SO_4)_2(OH)_6$) was confirmed by Favreau et al[31] in
288 altered zones of the outcrop, and Tl-rich jarosite formed via the substitution of K by Tl[44–46] has been
289 reported. This may also be the case in soils at the Jas Roux site, as confirmed below.
290 Similarities in the Mn and Zn maps were confirmed by the 2D intensity diagram and the high Pearson
291 coefficient. The high correlation could be attributed to the presence of phyllomanganate minerals such
292 as birnessite (δMnO_2) or chalcophanite ($ZnMn_3O_7.3H_2O$). Even if not detected via XRD, such minerals
293 are ubiquitous in soils[47] and can control the redox state of other metals and metalloids[48] such as Fe and
294 Tl as proposed below.
295 Micro-XRF only provided qualitative information due to the high spatial heterogeneity, and the
296 previous chemical map is only presented to suggest possible Tl-bearing phases. The following XAS
297 analyses further identified and quantified the Tl bearing phases and speciation.

298 **3) Tl(I) -jarosite/dorallcharite as major soilborne Tl-bearing minerals**

299 XAS spectra of the soil samples all exhibited a white line at 12672.5 eV, in the Tl(I) energy range
300 (Figure 4C). A feature/shoulder at 12678 eV (arrow A, Figure 4C) was also specific to the soil spectra.
301 The spectra of the three soils at the top of the toposequence appeared to be very similar, whereas
302 significant differences were noted in soils at the bottom, as shown in Figure 4C and 4D, especially at
303 12720eV.
304 Qualitatively the XAS spectra of the four soils highly resembled that of Tl-jarosite and differed
305 markedly from Tl sulfide primary minerals such as chabourneite or TlS.
306

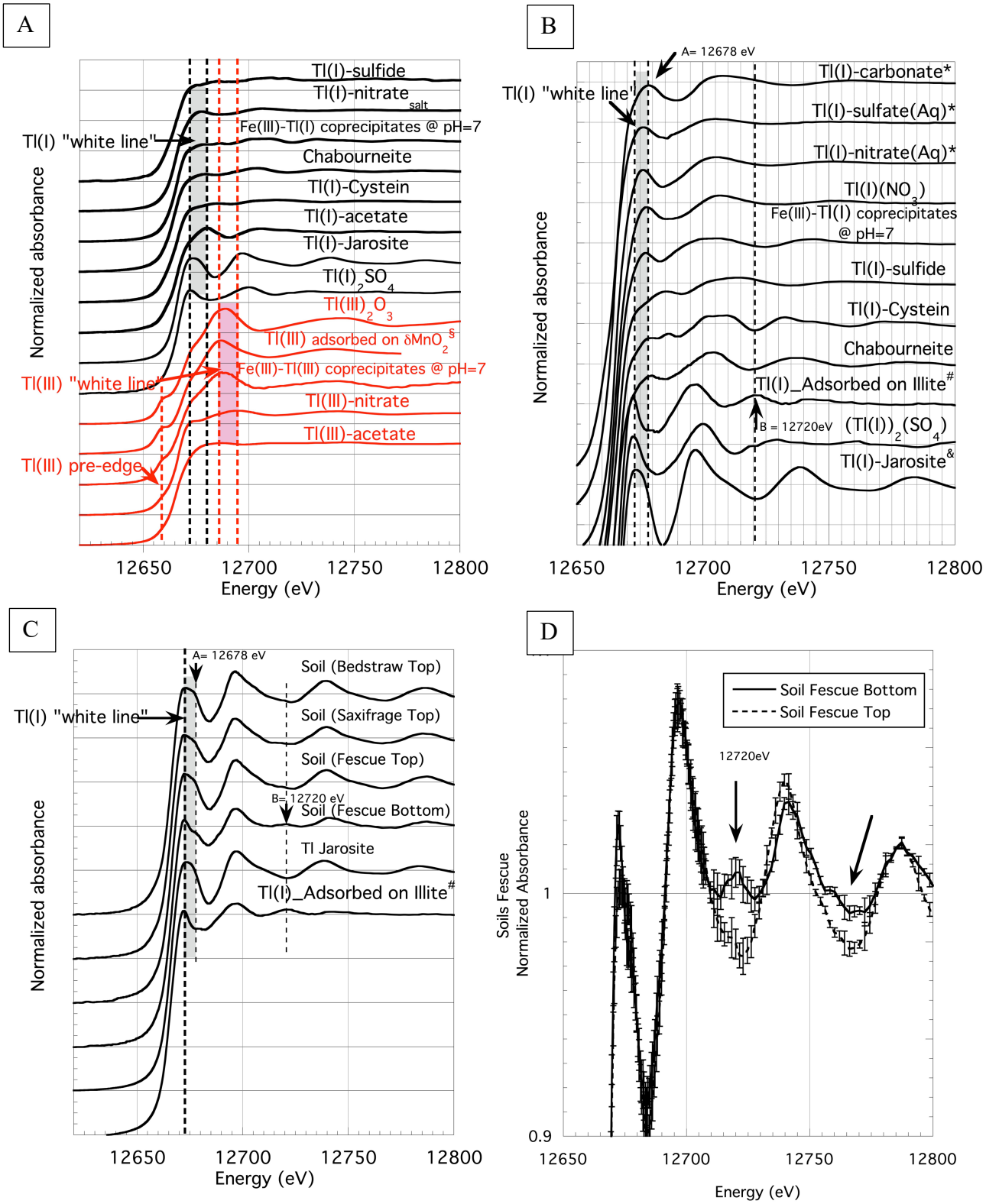

Figure 4: XAS spectra of: A) comparison between Tl^{1+} (black curves) and Tl^{3+} (red curves) reference compounds; B) full list of Tl^{1+} reference compounds for comparison; C) soil samples. Reference spectra from §[49], *[50], # [6], &[5] D) comparison of XAS spectra of bottom samples, including the variability level (error bars).

LCF was used to estimate the amount of Tl(I)-jarosite, but this technique, although efficient, has some limitations. Beyond the intrinsic sensitivity of the technique, i.e. ± 5 to 20%[43] in some cases, it

315 was impossible to choose among several fits because no significant differences in their residues were
316 noted. In the case of saxifrage and fescue soils, two fits were not distinguishable and are therefore just
317 presented as potential results. We found that Tl(I)-jarosite accounted for 93%±10%, 86-89% ±10%
318 and 67-82% ±10% of Tl speciation (Figures 5 & 6, Table S2) in the soil in the vicinity of bedstraw,
319 saxifrage and fescue plants, respectively, at the top of the toposequence. Tl-jarosite was previously
320 detected in the most altered zones of the outcrop[31] and our results corroborated its presence in soils
321 underlying the deposit. Other authors detected jarosite in soils with pH ranging from 6.2 to 7.2[5], which
322 is similar to the pH of the soils sampled at Jas Roux. Thermodynamic constants suggest that
323 dorallcharite and/or Tl-jarosite are more stable at pH > 5.5 compared to other Tl sulfate minerals such
324 as lanmuchangite[26]. The very high fraction of Tl found to be entrapped in Tl-jarosite therefore suggests
325 that in the vicinity of the sulfide deposit primary Tl-sulfide mineral oxidation would lead to the
326 formation of stable Tl-sulfate, in agreement with previous findings.

327 **4) Evidence of Tl(I) oxidation in Jas Roux soils**

328 For the fit of the soil in the vicinity of bedstraw plants at the top of the sequence, the use of a second
329 reference compound (7% of Tl(III) /Fe(III) coprecipitated at pH=7) decreased the residue by 40%
330 (Table S2) and the fit improvement was significantly higher than the variability of the soil XAS spectra
331 in the zone 12680-12700 eV (Figure S4). This strongly suggests the presence of Tl(III).

332 For the two other soils collected at the top (soils near fescue and saxifrage plants), the presence of
333 Tl-jarosite was > 67%, thereby highlighting that possible other phases could exist, such as Tl_2O_3 and/or
334 Tl(I)(NO_3) solid salt. Adding a second reference compound to Tl-jarosite decreased the residue.
335 However, the mathematical solutions were not unique since the absolute differences between the two
336 calculated spectra using two reference compounds, i.e. Fits 1 and 2 (Figures 5 & 6), were lower than
337 the XAS signal variability. In topsoil in the vicinity of saxifrage plants, the two indistinguishable fits
338 includes Tl(III) reference compounds, thereby strongly suggesting the presence of this element. The

Tl(III) presence could not be confirmed for the fescue soil since only one of the two indistinguishable fits included one Tl(III) reference compound (Table S2). For the soil at the bottom, the fit using three reference compounds (Tl-jarosite 47%, Tl adsorbed on illite 43% and Tl(III)$(NO_3)_3$ 10%) also suggested the presence of Tl(III) (Figure 6).

Although not confirmed for all of the soil samples, Tl(III) was likely present in the soils below the deposit. Jia et al.[51] suggested the possible oxidation of Tl(I) to Tl(III) by MnO_2 in soils, as noted in synthetic systems. Indeed, Bidoglio et al. observed surface precipitation of Tl_2O_3 resulting from Tl(I) adsorption on δ-MnO_2(s) and oxidation at the mineral surface. In a soil fraction from the Erzmatt site (Switzerland), Voegelin et al.[5] observed that up to 80% of Tl was absorbed as Tl(III) on birnessite and Tl_2O_3. The presence of Tl(III) in the soils below the Jas Roux deposit might be explained by the presence of Mn minerals, as revealed by the micro-XRF map (Figure 3), thereby causing Tl oxidation.

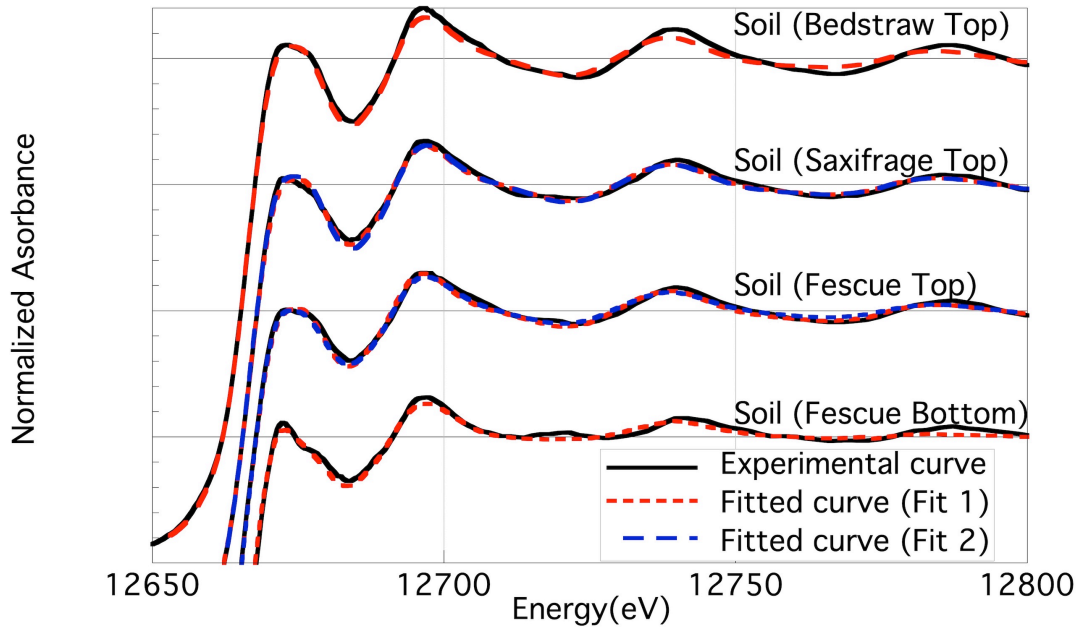

Figure 5: *XAS spectra of the soils. Dotted lines represent reconstructed spectra using LCF (red = fit 1, blue = fit 2).*

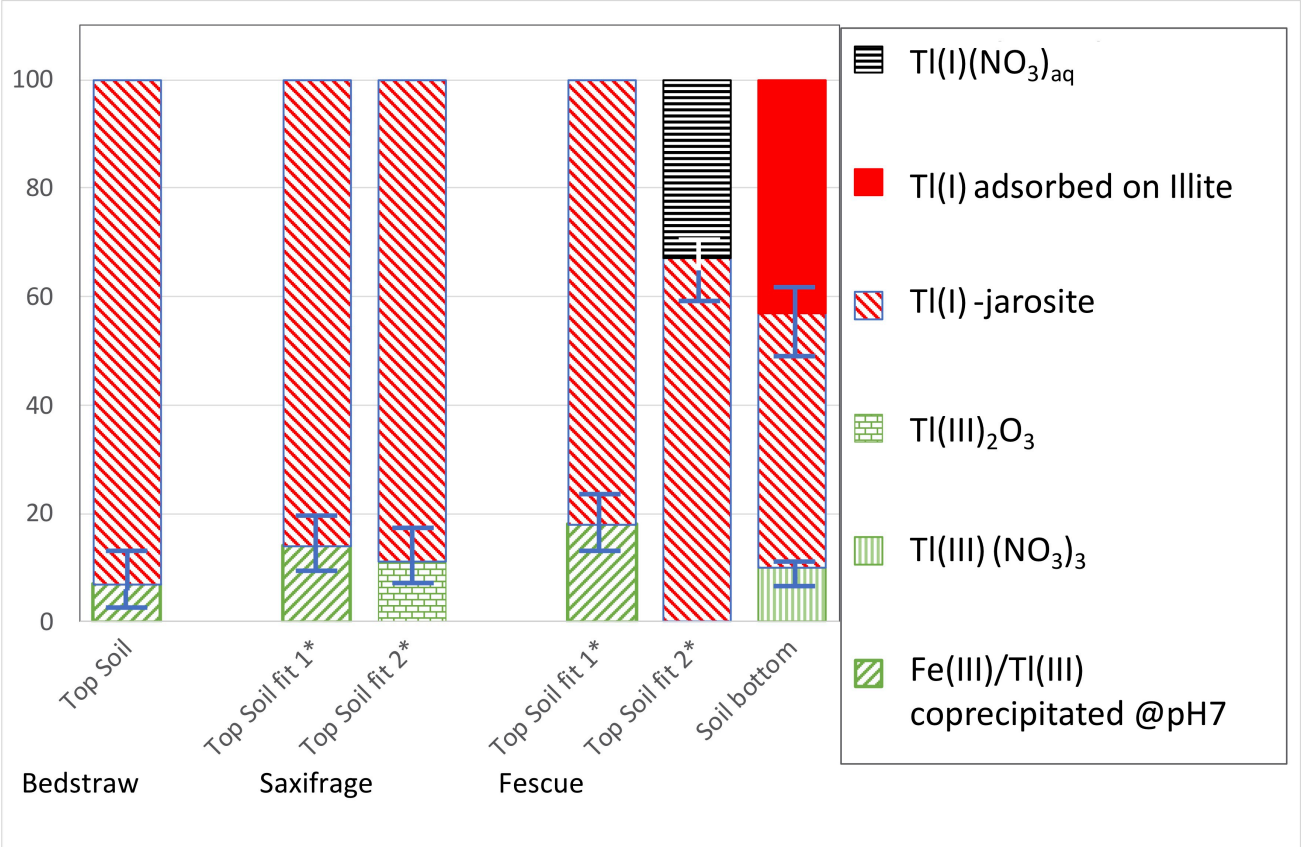

Figure 6: *Quantitative analysis of XAS data using LCF. *= fits with similar statistical significance levels.*

5) Tl(I)- silicate as a possible consequence of a Tl-jarosite decrease at the bottom of the toposequence.

One of the main interests of the Jas Roux site is that the Tl content in soils decreased from the top to the bottom of the toposequence. With distance from the source along the toposequence, oxidation of primary sulfide minerals may no longer be the only mechanism and other geochemical transformations may take place. This could therefore enhance the overall understanding of the long-term transfer and transformation of Tl at polluted sites.

The XAS spectrum fit obtained for soil at the bottom of the toposequence, suggested that Tl(I)-jarosite was main component (47%±10%), but its amount was significantly lower than that noted in soils at the top. This difference could be explained by partial dissolution of Tl(I)-jarosite and the formation of other secondary minerals such as FeOOH amorphous phases. Released Tl may either coprecipitate with FeOOH or adsorb at the surface of phyllosilicates such as muscovite or illite. The XAS fit of the spectrum favored the second hypothesis (Figure 6), with 43% (±10%) of Tl being

adsorbed on phyllosilicate. The presence of Tl adsorbed on phyllosilicate was also noted in soils sampled at the Erzmatt site[5].

6) Tl long-term transfer and transformation in soils

Our results provide valuable information indicating possible long-term Tl speciation changes in polluted areas. The unique feature of the Jas Roux site is that soils can be sampled at various distances from the Tl source in the outcrop. The soilborne primary sulfide and secondary sulphate contents were found to decrease with the distance from the outcrop. Indeed, the amount of sulfide minerals decreased from the top to the bottom of the toposequence, as suggested by the decrease in Fe (a major pyrite component), Zn (the main component of sphalerite) and also Pb and Ag (which were present in the form of sulfosalts in the outcrop). Note also that secondary sulfate mineral contents might have been lower at the bottom, as suggested by the decrease in Ba, which was mainly present in the form of Ba-sulfate minerals. Moreover, the Tl speciation pattern evolved from Tl-jarosite being a major component of soils at the top of the toposequence to a mix of Tl-jarosite and Tl adsorbed on phyllosilicate at the bottom. Tl(III) was also detected but there was no clearcut specific top-down evolution pattern.

CONCLUSION

The Tl speciation pattern in soils underlying the Jas Roux deposit was assessed for the first time. The results revealed that the Tl and Ba concentrations in the soils was high compared average soil values, as described by Kabata-Pendias[2]. A chemical gradient was found in soils from the top to the bottom of the studied zones below the Jas Roux outcrop. Using XAS, Tl was mainly found at the top of the toposequence in secondary minerals formed by oxidation and dissolution of Tl-rich sulfide minerals and reprecipitation of Tl(I)-jarosite, i.e. a stable Tl iron sulfate. The Tl(I)-jarosite content decreased at the bottom of the toposequence, with the possible release of Tl(I) and its adsorption at the

phyllosilicate surface. Although Tl(I)-jarosite was dominant, a decrease of sulfate at the bottom of the toposequence might have led to Tl-jarosite dissolution, a pattern that has not yet been clearly documented at contaminated sites. Tl adsorption on phyllosilicate that we identified at the Jas Roux site may represent another possible means of long-term Tl retention in soils. Note also that a fraction of Tl (7-18%) could exist in its Tl(III) oxidized form. Mn minerals may be involved in Tl oxidation, although there was no clear evidence of this at the Jas Roux site.

ACKNOWLEDGMENTS

We thank Ecrins National Park authorities for the sampling permission and their collaborative support. We are grateful to ESRF for providing access to the Synchrotron radiation facilities. The authors greatly thank Drs. Kirk Scheckel and Andreas Voegelin for valuable scientific input and for sharing the Tl reference compound XAS spectra. We are also grateful to Georges Favreau for sharing chabourneite compounds and expertise on the Jas Roux site. The Jas Roux site is located in Ecrins National Park. Sample collection is strictly forbidden, except in cases of special waivers, which must be authorized in advance by the park administration. Any offender is liable to serious penalties.

CORRESPONDING AUTHOR

Jérôme Rose

CEREGE, CNRS, Aix-Marseille Univ, IRD, INRAE

Avenue Louis Philibert, BP-80, 13545 Aix-en-Provence, cedex 4, France

rose@cerege.fr

Author Contributions

The manuscript was written on the basis of contributions of all authors. All authors have given approval to the final version of the manuscript.

Funding Sources

The research was funded by the ECosystèmes COntinentaux et Risques EnVironnementaux (ECCOREV, CNRS–Aix Marseille University, France) through the TRANSPLANTECH (TRANSferts solPLANTe d'éléments métalliques "high TECH") project. This work benefited from the MATRIX platform (CEREGE, France), funded by the French "Investissements d'Avenir" program managed by the French National Research Agency through Nano-ID (EQUIPEX ANR-10-EQPX39-01) and IMAGINE^2 (EQUIPEX ANR-21-ESRE-0043). Matrix is member of the REGEF French research infrastructure. This research is also a contribution to OSU-Institut Pythéas. The authors thank CNRS for funding the project IRP iNOVE.

REFERENCES

(1) Jambor, J. L.; Nordstrom, D. K.; Alpers, C. N. Metal-Sulfate Salts from Sulfide Mineral Oxidation. *Rev. Mineral. Geochem.* **2000**, *40* (1), 303–350. https://doi.org/10.2138/rmg.2000.40.6.
(2) Kabata-Pendias, A. *Trace Elements in Soils and Plants, Fourth Edition*; CRC Press, 2010. https://doi.org/10.1201/b10158.
(3) Tremel, A.; Masson, P.; Sterckeman, T.; Baize, D.; Mench, M. Thallium in French Agrosystems .1. Thallium Contents in Arable Soils. *Environ. Pollut.* **1997**, *95* (3), 293–302. https://doi.org/10.1016/s0269-7491(96)00145-5.
(4) Zhao, F.; Gu, S. Secondary Sulfate Minerals from Thallium Mineralized Areas: Their Formation and Environmental Significance. *Minerals* **2021**, *11* (8), 855. https://doi.org/10.3390/min11080855.
(5) Voegelin, A.; Pfenninger, N.; Petrikis, J.; Majzlan, J.; Plötze, M.; Senn, A.-C.; Mangold, S.; Steininger, R.; Göttlicher, J. Thallium Speciation and Extractability in a Thallium- and Arsenic-Rich Soil Developed from Mineralized Carbonate Rock. *Environ. Sci. Technol.* **2015**, *49* (9), 5390–5398. https://doi.org/10.1021/acs.est.5b00629.
(6) Wick, S.; Baeyens, B.; Fernandes, M. M.; Voegelin, A. Thallium Adsorption onto Illite. *Environ. Sci. Technol.* **2018**, *52* (2), 571–580. https://doi.org/10.1021/acs.est.7b04485.
(7) Baceva, K.; Stafilov, T.; Sajn, R.; Tanaselia, C.; Makreski, P. Distribution of Chemical Elements in Soils and Stream Sediments in the Area of Abandoned Sb-As-Tl Allchar Mine, Republic of Macedonia. *Environ. Res.* **2014**, *133*, 77–89. https://doi.org/10.1016/j.envres.2014.03.045.
(8) Hettmann, K.; Kreissig, K.; Rehkämper, M.; Wenzel, T.; Mertz-Kraus, R.; Markl, G. Thallium Geochemistry in the Metamorphic Lengenbach Sulfide Deposit, Switzerland: Thallium-Isotope Fractionation in a Sulfide Melt. *Am. Mineral.* **2014**, *99* (4), 793–803. https://doi.org/10.2138/am.2014.4591.
(9) Xiao, T. F.; Guha, J.; Boyle, D.; Liu, C. Q.; Chen, J. G. Environmental Concerns Related to High Thallium Levels in Soils and Thallium Uptake by Plants in Southwest Guizhou, China. *Sci.*

Total Environ. **2004**, *318* (1–3), 223–244. https://doi.org/10.1016/S0048-9697(03)00448-0.
(10) Xiao, T. F.; Guha, J.; Boyle, D.; Liu, C. Q.; Zheng, B. S.; Wilson, G. C.; Rouleau, A.; Chen, J. Naturally Occurring Thallium: A Hidden Geoenvironmental Health Hazard? *Environ. Int.* **2004**, *30* (4), 501–507. https://doi.org/10.1016/j.envint.2003.10.004.
(11) Johan, Z.; Mantienne, J. Thallium-Rich Mineralization at Jas Roux, Hautes-Alpes, France: A Complex Epithermal, Sediment-Hosted, Ore-Forming System. *Journal of the Czech Geological Societey*. 2000, pp 63–77.
(12) Sankar, C. R.; Assoud, A.; Kleinke, H. New Layered-Type Quaternary Chalcogenides, Tl(2)PbMQ(4) (M = Zr, Hf; Q = S, Se): Structure, Electronic Structure, and Electrical Transport Properties. *Inorg. Chem.* **2013**, *52* (24), 13869–13874. https://doi.org/10.1021/ic4025316.
(13) Abd-Shukor, R. Ultrasonic and Elastic Properties of Tl- and Hg-Based Cuprate Superconductors: A Review. *Phase Transit.* **2018**, *91* (1), 48–57. https://doi.org/10.1080/01411594.2017.1357181.
(14) Agarwal, A.; Vishnoi, A. N. XANES Studies of Thallium Compounds and Valence States and Local Environment of Thallium in Some of Its Superconducting Cuprates. *Phys. Scr.* **2005**, *T115*, 534–537.
(15) Fang, M.-H.; Wang, H.-D.; Dong, C.-H.; Li, Z.-J.; Feng, C.-M.; Chen, J.; Yuan, H. Q. Fe-Based Superconductivity with T-C=31 K Bordering an Antiferromagnetic Insulator in (Tl,K) FexSe2. *Epl* **2011**, *94* (2), 27009. https://doi.org/10.1209/0295-5075/94/27009.
(16) Moeinian, M.; Akhbari, K. Various Methods for Synthesis of Bulk and Nano Thallium(III) Oxide. *J. Inorg. Organomet. Polym. Mater.* **2016**, *26* (1), 1–13. https://doi.org/10.1007/s10904-015-0289-z.
(17) Kurosaki, K.; Li, G.; Ohishi, Y.; Muta, H.; Yamanaka, S. Enhancement of Thermoelectric Efficiency of CoSb3-Based Skutterudites by Double Filling with K and TI. *Front. Chem.* **2014**, *2*, 84. https://doi.org/10.3389/fchem.2014.00084.
(18) Kazantzis, G. Thallium in the Environment and Health Effects. *Environ. Geochem. Health* **2000**, *22* (4), 275–280. https://doi.org/10.1023/a:1006791514080.
(19) Heim, M.; Wappelhorst, O.; Markert, B. Thallium in Terrestrial Environments - Occurrence and Effects. *Ecotoxicology* **2002**, *11* (5), 369–377. https://doi.org/10.1023/a:1020513523462.
(20) Peter, A. L. J.; Viraraghavan, T. Thallium: A Review of Public Health and Environmental Concerns. *Environ. Int.* **2005**, *31* (4), 493–501. https://doi.org/10.1016/j.envint.2004.09.003.
(21) Krasnodebska-Ostrega, B.; Sadowska, M.; Ostrowska, S. Thallium Speciation in Plant Tissues-Tl(III) Found in Sinapis Alba L. Grown in Soil Polluted with Tailing Sediment Containing Thallium Minerals. *Talanta* **2012**, *93*, 326–329. https://doi.org/10.1016/j.talanta.2012.02.042.
(22) Krasnodebska-Ostrega, B.; Asztemborska, M.; Golimowski, J.; Strusinska, K. Determination of Thallium Forms in Plant Extracts by Anion Exchange Chromatography with Inductively Coupled Plasma Mass Spectrometry Detection (IC-ICP-MS). *J. Anal. At. Spectrom.* **2008**, *23* (12), 1632–1635. https://doi.org/10.1039/b804456b.
(23) Ospina-Alvarez, N.; Burakiewicz, P.; Sadowska, M.; Krasnodebska-Ostrega, B. Tl-I and Tl-III Presence in Suspended Particulate Matter: Speciation Analysis of Thallium in Wastewater. *Environ. Chem.* **2015**, *12* (3), 374–379. https://doi.org/10.1071/EN14181.
(24) Sadowska, M.; Biadun, E.; Krasnodebska-Ostrega, B. Stability of TI(III) in the Context of Speciation Analysis of Thallium in Plants. *Chemosphere* **2016**, *144*, 1216–1223. https://doi.org/10.1016/j.chemosphere.2015.09.079.
(25) Yao, Y.; Zhang, F.; Wang, M.; Liu, F.; Liu, W.; Li, X.; Qin, D.; Geng, X.; Huang, X.; Zhang, P. Thallium-Induced Oxalate Secretion from Rice (Oryza Sativa L.) Root Contributes to the Reduction of Tl(III) to Tl(I). *Environ. Exp. Bot.* **2018**, *155*, 387–393. https://doi.org/10.1016/j.envexpbot.2018.07.028.
(26) Xiong, Y. The Aqueous Geochemistry of Thallium: Speciation and Solubility of Thallium in

Low Temperature Systems. *Environ. Chem.* 2009, pp 441–451.
(27) Biagioni, C.; D'Orazio, M.; Lepore, G. O.; d'Acapito, F.; Vezzoni, S. Thallium-Rich Rust Scales in Drinkable Water Distribution Systems: A Case Study from Northern Tuscany, Italy. *Sci. Total Environ.* **2017**, *587*, 491–501. https://doi.org/10.1016/j.scitotenv.2017.02.177.
(28) Liu, J.; Luo, X.; Sun, Y.; Tsang, D. C. W.; Qi, J.; Zhang, W.; Li, N.; Yin, M.; Wang, J.; Lippold, H.; Chen, Y.; Sheng, G. Thallium Pollution in China and Removal Technologies for Waters: A Review. *Environ. Int.* **2019**, *126*, 771–790. https://doi.org/10.1016/j.envint.2019.01.076.
(29) Wierzbicka, M.; Szarek-Łukaszewska, G.; Grodzińska, K. Highly Toxic Thallium in Plants from the Vicinity of Olkusz (Poland). *Ecotoxicol. Environ. Saf.* **2004**, *59* (1), 84–88. https://doi.org/10.1016/j.ecoenv.2003.12.009.
(30) Mantienne, J. La Minéralisation Thallifère de Jas Roux (Hautes-Alpes). Manuscript, Université Pierre et Marie Curie - Paris VI, Paris France, 1974.
(31) Favreau, G.; Bourgoin, V.; Bouillard, jean-C. *Géologie et Minéralogie Du Gisement de Minéraux de Thallium de Jas Roux*; Le Cahier des micromonteurs; Association Française de Microminéralogie, 2011; Vol. 113.
(32) Topa, D.; Makovicky, E.; Favreau, G.; Bourgoin, V.; Boulliard, J.-C.; Zagler, G.; Putz, H. Jasrouxite, a New Pb–Ag–As–Sb Member of the Lillianite Homologous Series from Jas Roux, Hautes-Alpes, France. *Eur. J. Mineral.* **2013**, *25* (6), 1031–1038. https://doi.org/10.1127/0935-1221/2013/0025-2336.
(33) Biagioni, C.; Moelo, Y.; Favreau, G.; Bourgoin, V.; Boulliard, J.-C. Structure of Pb-Rich Chabourneite from Jas Roux, France. *Acta Crystallogr. Sect. B-Struct. Sci. Cryst. Eng. Mater.* **2015**, *71*, 81–88. https://doi.org/10.1107/S2052520614028157.
(34) Johan, Z.; Mantienne, J.; Picot, P. Chabourneite, a New Thallium Mineral. *Bull. Mineral.* **1981**, *104* (1), 10–15. https://doi.org/10.3406/bulmi.1981.7538.
(35) Fehlauer, T.; Collin, B.; Angeletti, B.; Santaella, C.; Dentant, C.; Chaurand, P.; Levard, C.; Gonneau, C.; Borschneck, D.; Rose, J. Uptake Patterns of Critical Metals in Alpine Plant Species Growing in an Unimpaired Natural Site. *Chemosphere* **2022**, *287*, 132315. https://doi.org/10.1016/j.chemosphere.2021.132315.
(36) Tricart, P. From Extension to Transpression during the Final Exhumation of the Pelvoux and Argentera Massifs, Western Alps. *Eclogae Geol. Helvetiae* **2004**, *97* (3), 429–439. https://doi.org/10.1007/s00015-004-1138-1.
(37) Delunel, R. Evolution Géomorphologique Du Massif Des Ecrins-Pelvoux Depuis Le Dermier Maximum Glaciaire – Apports Des Nucléides Cosmogéniques Produits in-Stu, 2010.
(38) A.F.N.O.R. NF ISO 10390 Soil Quality - Détermination of pH. *NF ISO*. 2005.
(39) Schindelin, J.; Arganda-Carreras, I.; Frise, E.; Kaynig, V.; Longair, M.; Pietzsch, T.; Preibisch, S.; Rueden, C.; Saalfeld, S.; Schmid, B.; Tinevez, J.-Y.; White, D. J.; Hartenstein, V.; Eliceiri, K.; Tomancak, P.; Cardona, A. Fiji: An Open-Source Platform for Biological-Image Analysis. *Nat. Methods* **2012**, *9* (7), 676–682. https://doi.org/10.1038/nmeth.2019.
(40) Proux, O.; Lahera, E.; Del Net, W.; Kieffer, I.; Rovezzi, M.; Testemale, D.; Irar, M.; Thomas, S.; Aguilar-Tapia, A.; Bazarkina, E. F.; Prat, A.; Tella, M.; Auffan, M.; Rose, J.; Hazemann, J.-L. High-Energy Resolution Fluorescence Detected X-Ray Absorption Spectroscopy: A Powerful New Structural Tool in Environmental Biogeochemistry Sciences. *J. Environ. Qual.* **2017**, *46* (6), 1146–1157. https://doi.org/10.2134/jeq2017.01.0023.
(41) Ravel, B.; Newville, M. ATHENA, ARTEMIS, HEPHAESTUS: Data Analysis for X-Ray Absorption Spectroscopy Using IFEFFIT. *J. Synchrotron Radiat.* **2005**, *12*, 537–541. https://doi.org/10.1107/s0909049505012719.
(42) Michalowicz, A.; Moscovici, J.; Muller-Bouvet, D.; Provost, K. MAX (Multiplatform Applications for XAFS) New Features. *J. Phys. Conf. Ser.* **2013**, *430* (1), 012016. https://doi.org/10.1088/1742-6596/430/1/012016.

(43) O'Day, P. A.; Rivera, N.; Root, R.; Carroll, S. A. X-Ray Absorption Spectroscopic Study of Fe Reference Compounds for the Analysis of Natural Sediments. *Am. Mineral.* **2004**, *89* (4), 572–585.
(44) Aguilar-Carrillo, J.; Herrera-Garcia, L.; Reyes-Dominguez, I. A.; Gutierrez, E. J. Thallium(I) Sequestration by Jarosite and Birnessite: Structural Incorporation vs Surface Adsorption. *Environ. Pollut.* **2020**, *257*, 113492. https://doi.org/10.1016/j.envpol.2019.113492.
(45) BalicZunic, T.; MOELO, Yves.; Loncar, Z.; Micheelsen, H. Dorallcharite : Ti0.8K0.2Fe3(SO4)2(OH)6, a New Member of the Jarosite-Alunite Family. *Eur. J. Mineral.* **1994**, *6*, 255–263.
(46) Dutrizac, J. E. The Behavior of Thallium during Jarosite Precipitation. *Metall. Mater. Trans. B-Process Metall. Mater. Process. Sci.* **1997**, *28* (5), 765–776. https://doi.org/10.1007/s11663-997-0003-9.
(47) Grangeon, S.; Lanson, B.; Lanson, M. Solid-State Transformation of Nanocrystalline Phyllomanganate into Tectomanganate: Influence of Initial Layer and Interlayer Structure. *Acta Crystallogr. Sect. B-Struct. Sci. Cryst. Eng. Mater.* **2014**, *70*, 828–838. https://doi.org/10.1107/S2052520614013687.
(48) Vanek, A.; Komarek, M.; Vokurkova, P.; Mihaljevic, M.; Sebek, O.; Panuskova, G.; Chrastny, V.; Drabek, O. Effect of Illite and Birnessite on Thallium Retention and Bioavailability in Contaminated Soils. *J. Hazard. Mater.* **2011**, *191* (1–3), 170–176. https://doi.org/10.1016/j.jhazmat.2011.04.065.
(49) Wick, S.; Pena, J.; Voegelin, A. Thallium Sorption onto Manganese Oxides. *Environ. Sci. Technol.* **2019**, *53* (22), 13168–13178. https://doi.org/10.1021/acs.est.9b04454.
(50) Scheckel, K. G.; Lombi, E.; Rock, S. A.; McLaughlin, M. J. In Vivo Synchrotron Study of Thallium Speciation and Compartmentation in Lberis Intermedia. *Environ. Sci. Technol.* **2004**, *38* (19), 5095–5100. https://doi.org/10.1021/es049569g.
(51) Jia, Y.; Xiao, T.; Zhou, G.; Ning, Z. Thallium at the Interface of Soil and Green Cabbage (Brassica Oleracea L. Var. Capitata L.): Soil-Plant Transfer and Influencing Factors. *Sci. Total Environ.* **2013**, *450*, 140–147. https://doi.org/10.1016/j.scitotenv.2013.02.008.
(52) Bidoglio, G.; Gibson, P.; Ogorman, M.; Roberts, K. X-Ray-Absorption Spectroscopy Investigation of Surface Redox Transformations of Thallium and Chromium on Colloidal Mineral Oxides. *Geochim. Cosmochim. Acta* **1993**, *57* (10), 2389–2394. https://doi.org/10.1016/0016-7037(93)90576-I.

Supporting information

Table S1 lists all the reference compounds used in XAS analysis. Table S2 details the quantitative parameters used in EXAFS spectra modeling, illustrated in figure 6. Figure S1 shows the rock outcrop and its various oxidized and slightly weathered zones. Figure S2 shows X-ray fluorescence spectra acquired on site using a portable spectrometer, illustrating the differences between the weathered zones of the outcrop and the underlying soils. Figure S3 shows the results of the statistical analysis of the spectra, which indicates the number of spectra that can be used in the linear combination analysis. Figure S4 shows the difference between two XAS models and the signal-to-noise level.